Nuclear matter properties from a separable representation of the Paris interaction

M. Baldo, I. Bombaci, G. Giansiracusa, and U. Lombardo
Dipartimento di Fisica, Università di Catania, and Istituto Nazionale di Fisica Nucleare, Sezione di Catania, Corso Italia, 57, I-95129 Catania, Italy

C. Mahaux and R. Sartor
Institut de Physique B5, Université de Liège, B-4000 Liège 1, Belgium
(Received 5 October 1989)

A separable representation of the Paris interaction is used as input for the investigation of various nuclear matter properties. The faithfulness of the separable representation is checked by comparison with results previously obtained from the original Paris interaction. Calculations are performed for four different values of the Fermi momentum, namely $k_F = 1.10$, 1.36, 1.55, and 1.75 fm^{-1}. One evaluates the contributions to the quasiparticle potential energy that are of first, second, and third order in the reaction matrix. The momentum distribution $n(k)$ in the correlated ground state is calculated up to second order in the reaction matrix. For $0 < k < 2$ fm^{-1}, it mainly depends upon the ratio k/k_F; in the domain $2 < k < 4.5$ fm^{-1}, it is accurately reproduced by the expression $\frac{1}{7}k_F^5 e^{-1.6k}$, with k and k_F in units of fm^{-1}. The quasiparticle strength at the Fermi surface is calculated, as well as the mean-square deviation of the one-body density matrix from that of the unperturbed Fermi sea: This quantity gives an estimate of the minimum value of the norm of the difference between the one-body density matrix of a correlated nucleus and that associated with any Slater determinant. The average kinetic energy per nucleon is evaluated. Various contributions to the average binding energy per nucleon are investigated in the framework of Brueckner's expansion; particular attention is paid to the dependence of the calculated binding energy upon the choice of the "auxiliary" potential which is added to and subtracted from the Hamiltonian before performing the expansion. One also evaluates diagrams that are characteristic of the difference between the Green's function and the Brueckner hole-line expansions. The fulfillment of the Hugenholtz–Van Hove theorem is studied.

I. INTRODUCTION

Sizable differences persist between various calculations of nuclear matter properties.[1] This reflects the difficulty of the problem, due to the strong and complicated nature of the nucleon-nucleon interaction. The computations are quite time consuming even in the lowest-order approximation. They become somewhat prohibitive when one wants to evaluate higher-order corrections; the latter are quite instructive since the accuracy of an approximation should be estimated from the magnitude of the higher-order terms that have been neglected.[2] It is therefore of particular interest to use realistic nucleon-nucleon interactions whose functional form is well adapted to a fast and accurate evaluation of the lowest-order contribution. In the case of Brueckner's and related approaches to nuclear matter, this amounts to considering an interaction for which the reaction matrix can be calculated by algebraic means. This is the case for a separable interaction.[3,4] In this work we use the separable interaction of Haidenbauer and Plessas,[5] which closely reproduces the Paris nucleon-nucleon potential.[6] We shall argue that this separable approximation is sufficiently faithful for a meaningful investigation of several nuclear matter properties, which we now enumerate while describing our presentation.

Section II is devoted to the potential energy of a quasiparticle: We evaluate the Brueckner-Hartree-Fock (BHF), the second order and one of the third order (in the reaction matrix) contributions to the mass operator, up to a momentum equal to 4.5 fm^{-1} and for four different values of the Fermi momentum, namely $k_F = 1.10$, 1.36, 1.55, and 1.75 fm^{-1}.

The interaction among the nucleons implies that the Fermi sea is partly depleted, and that momentum states larger than k_F are partly occupied. The momentum distribution is of manifold interest. It is computed and parametrized in Sec. III. We compare our results with the few previous calculations of this quantity. Since states with momentum larger than k_F are occupied in the correlated ground state, the average kinetic energy per nucleon is larger for the correlated than for the uncorrelated system; it is calculated in Sec. IV.

In the nuclear shell model, it is assumed that the ground-state wave function is a Slater determinant. The goodness of this model depends upon the observable that is considered. The one-body density matrix is of particular interest. The norm of the square of the difference between the actual and the shell-model one-body density matrices depends upon the choice of the single-particle orbits. It cannot be smaller than a minimum value, which we compute in Sec. V in the case of nuclear matter.

Section VI is devoted to the average binding energy per

nucleon, that is the quantity on which attention has been focused in most previous papers. We consider Brueckner-type expansions. They involve an "auxiliary" one-body potential $U(k)$, which is added to and subtracted from the Hamiltonian before performing the expansion. One tries to choose it in such a way that the rate of convergence of the expansion is optimized. The "standard choice" consists in identifying $U(k)$ with the BHF potential energy for $k<k_F$ and in setting $U(k)=0$ for $k>k_F$; this standard choice is used in the Appendix to check the faithfulness of the separable representation of the Paris interaction. It is appropriate neither to the inclusion of long-range correlations[7,8] nor to the calculation of nuclear matter properties other than the binding energy.[9,10] This has led to the use of "continuous choices" for which $U(k)$ is continuous at $k=k_F$. Here, we mainly consider the continuous choice for which $U(k)$ is identified with the BHF potential for all values of k (larger as well as smaller than k_F), but we also discuss another continuous choice. In addition, we evaluate diagrams that appear in a Brueckner-type expansion based on the Green's function approach.[11] In Sec. VII, we investigate to what extent our calculations fulfill the Hugenholtz-Van Hove theorem[12] which states, in particular, that at equilibrium the average binding energy per nucleon is equal to the energy of a quasiparticle with momentum k_F. Finally, Sec. VIII contains a summary and a discussion.

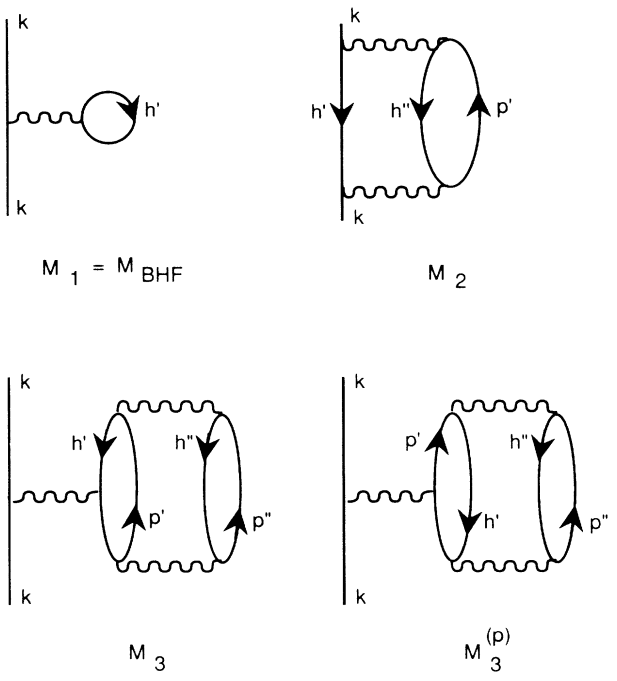

FIG. 1. Four contributions to the hole-line expansion of the mass operator. The diagram labeled M_1 represents the BHF approximation, that labeled M_2 the second-order contribution and that labeled M_3 the renormalization contribution; the diagram $M_3^{(p)}$ is not evaluated in this work. A wiggly horizontal line corresponds to a reaction matrix. The exchange diagrams are not shown, for simplicity.

II. QUASIPARTICLE POTENTIAL ENERGY

The quasiparticle energy can be identified with the on-the-energy-shell value of the mass operator, for which a Brueckner-type hole-line expansion exists.[9] Here, we shall evaluate the contributions M_1, M_2, and M_3 of Fig. 1. We set $\hbar=1$.

A. BHF approximation

Let $U(k)$ denote the "auxiliary" potential energy associated with a nucleon with momentum k and $e(k)$ the corresponding energy:

$$e(k)=\frac{k^2}{2m}+U(k)\ . \tag{2.1}$$

The word "auxiliary" emphasizes that $U(k)$ does not need to have any physical meaning. Brueckner's reaction matrix is the solution of the following integral equation:

$$g[w]=v+v\sum_{p,p'}\frac{|pp'\rangle\langle pp'|}{w-e(p)-e(p')+i\delta}g[w]\ . \tag{2.2}$$

Here, the labels $p,p',\ldots$ refer to "particle" plane-wave states, with momenta larger than the Fermi momentum k_F. In the following, the labels $h,h',\ldots$ will denote "hole" states, with momenta smaller than k_F; the label k will correspond to particle as well as to hole states. The operator $g[w]$ depends on a parameter w, which always has to be specified. We only deal with real quantities, and omit the $+i\delta$ in the denominator on the right-hand side of (2.2); there and in the following the summations will be defined as principal value integrals whenever the integrand involves a denominator that vanishes in the range of integration.

The BHF approximation to the quasiparticle potential is represented by the diagram labeled M_1 in Fig. 1. Its algebraic expression reads

$$M_1(k)=\sum_{h'}\langle kh'|g[e(k)+e(h')]|kh'\rangle\ . \tag{2.3}$$

Here and below the ket ($|kh'\rangle$ in this case) in any matrix element is antisymmetrized. The choice of $U(k)$ must still be specified. Unless otherwise stated, we adopt the following BHF "continuous choice:"

$$U(k)=M_1(k)\ \text{ for all } k\ . \tag{2.4a}$$

This is a self-consistent prescription in the sense that the value of $U(k)$ depends on the value of $M_1(k)$, which itself depends on $U(k)$. Henceforth, we attach an index 1 to the quantities associated with this BHF approximation, e.g.,

$$e_1(k)=\frac{k^2}{2m}+M_1(k)\ . \tag{2.4b}$$

One of the advantages of the use of a separable interaction is that the computation of $M_1(k)$ is sufficiently fast to enable one to impose the self-consistency condition (2.4b) at values of k that are closely spaced (steps of 0.09 fm^{-1}) and extend up to large momenta (4.5 fm^{-1}). The calculated values of the BHF potential energy are represented by the dots in Fig. 2.

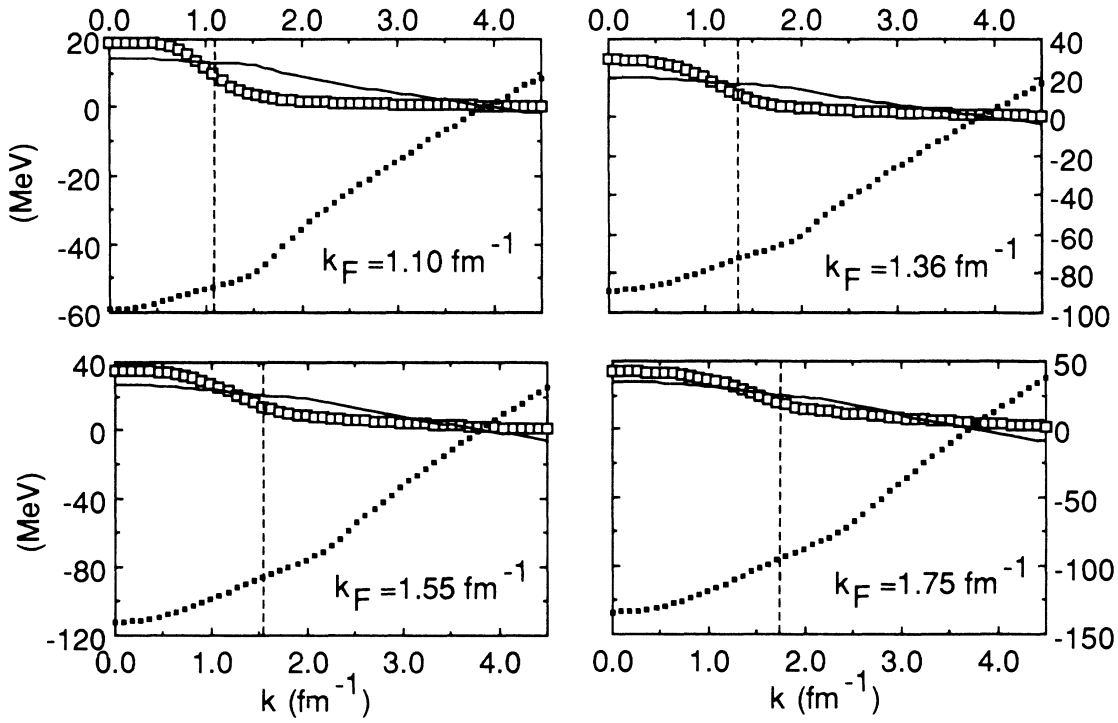

FIG. 2. The dots represent the BHF approximation $M_1(k)$ to the potential energy [Eq. (2.3)], the open squares the second-order contribution $M_2(k)$ [Eq. (2.5)], and the solid curve the renormalization contribution $M_3(k)$ [Eq. (2.11)], for $k_F=1.10$, 1.36, 1.55, and 1.75 fm^{-1}. The vertical dashed lines show the location of the Fermi surface. These results extend those previously published in Ref. 14.

B. Second-order contribution

The expression of the second-order diagram M_2 is the following:[13]

$$M_2(k)=\tfrac{1}{2}\sum_{h'h''p'}\frac{|\langle h'h''|g[e_1(h')+e_1(h'')]|kp'\rangle|^2}{e_1(k)+e_1(p')-e_1(h')-e_1(h'')} \quad (2.5)$$

This quantity is represented by the open squares in Fig. 2. These results are in good agreement with those published for $k_F=1.36$ fm^{-1} in Ref. 15, where the original Paris interaction was used. They are sizable for $k<k_F$, but decrease rapidly with increasing $k>k_F$; these features are common to the few calculations of $M_2(k)$, which had been performed previously.[3,14–17]

The sum $M_1(k)+M_2(k)$ should not be identified to the potential energy of a quasiparticle with momentum k, as we now discuss. The diagrams in Fig. 1 actually represent contributions to the mass operator, which depends upon the nucleon momentum k and upon its frequency ω. For instance, one has

$$\mathcal{M}_1(k;\omega)=\sum_h\langle kh|g[\omega+e_1(h)]|kh\rangle , \quad (2.6a)$$

$$\mathcal{M}_2(k,\omega)=\tfrac{1}{2}\sum_{h'h''p'}\frac{|\langle h'h''|g[e_1(h')+e_1(h'')]|kp'\rangle|^2}{\omega+e_1(p')-e_1(h')-e_1(h'')} . \quad (2.6b)$$

Note that

$$M_1(k)=\mathcal{M}_1(k;e_1(k)), \quad M_2(k)=\mathcal{M}_2(k;e_1(k)) . \quad (2.7)$$

The quasiparticle energy $E(k)$ is defined by the following energy-momentum relation:

$$E(k)=\frac{k^2}{2m}+\mathcal{M}(k;E(k)) . \quad (2.8)$$

In the BHF approximation, $\mathcal{M}$ is replaced by $\mathcal{M}_1$ and $E(k)$ is identical to $e_1(k)$.

When $\mathcal{M}_2$ is included, the quasiparticle energy is given by

$$E_{1+2}(k)=e_1(k)+\delta_2(k) , \quad (2.9a)$$

with

$$\delta_2(k)\approx Z_{1+2}(k)M_2(k) , \quad (2.9b)$$

where

$$Z_{1+2}(k)=\left\{1-\frac{\partial}{\partial\omega}[\mathcal{M}_1(k;\omega)+\mathcal{M}_2(k;\omega)]\right\}^{-1}_{\omega=e_1(k)} \quad (2.9c)$$

is an approximation to the "quasiparticle strength," namely to[13]

$$Z(k)=\left[1-\frac{\partial}{\partial\omega}\mathcal{M}(k,\omega)\right]^{-1}_{\omega=E(k)} . \quad (2.10)$$

Figure 3 shows that, for $k=k_F$, $Z_{1+2}(k)$ is as small as

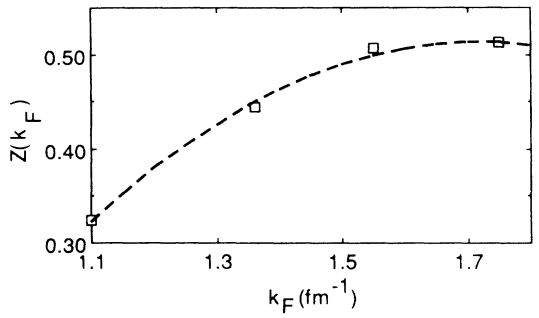

FIG. 3. Dependence of the quasiparticle strength upon the Fermi momentum, up to second order in the reaction matrix. The squares represent the calculated values; the dashed curve is a fit.

0.3–0.5; Eqs. (2.9a) and (2.9b) thus show that the second-order correction to the potential energy would be overestimated if one would take it equal to $M_1(k)+M_2(k)$; we return to this point in Sec. VII.

C. Renormalization contribution

When added to M_1, the graph M_3 yields the "renormalized BHF approximation." It accounts for the fact that the nucleon with momentum k cannot interact with the hole momentum state h' because the latter is not fully occupied in the *correlated* ground state. Its expression is given by[13]

$$\mathcal{M}_3(k;\omega)=-\sum_{h'}\kappa_2(h')\langle kh'|g[\omega+e_1(h')]|kh'\rangle \ , \tag{2.11}$$

where $\kappa_2(h')$ is the lowest-order contribution to the probability that the hole momentum state h' be empty, namely

$$\kappa_2(h')=\tfrac{1}{2}\sum_{h''p'p''}\frac{|\langle h'h''|g[e_1(h')+e_1(h'')]|p'p''\rangle|^2}{[e_1(h')+e_1(h'')-e_1(p')-e_1(p'')]^2} \tag{2.12a}$$

$$=-\left[\frac{\partial}{\partial\omega}\mathcal{M}_1(h';\omega)\right]_{\omega=e_1(h')} . \tag{2.12b}$$

The quantity $\kappa_2(h')$ will be calculated in Sec. III. We checked that a very accurate (1%) approximation consists in replacing in Eq. (2.11) the coefficient $\kappa_2(h')$ by its value κ at the average of h' in the Fermi sea, namely at $h'=0.75k_F$. Equation (2.11) then yields

$$M_3(k)=\mathcal{M}_3(k;e_1(k))\approx-\kappa M_1(k)=M_1^{(R)}(k) \ . \tag{2.13a}$$

The quantity $M_3(k)$ is represented by the solid curves in Fig. 2.

A renormalization correction should also be brought to the second-order contribution M_2 in order to take into account the fact that the hole momentum state h' is partly empty (see Fig. 1). This correlation is approximately equal to

$$M_2^{(R)}(k)\approx-\kappa M_2(k) \ . \tag{2.13b}$$

The sum $M_2+M_3+M_2^{(R)}$ can thus be approximated by

$$M_{2+3}^{(R)}(k)\approx-\kappa M_1(k)+(1-\kappa)M_2(k) \ . \tag{2.14}$$

It should be kept in mind that this quantity should not be identified with the correction to the potential energy of a nucleon with momentum k. Rather, this correction is approximately equal to $M_{2+3}^{(R)}(k)$ multiplied by the following factor [see Eq. (2.9c)]:

$$Z_{1+2+3}(k)\approx\left\{1-(1-\kappa)\frac{\partial}{\partial\omega}[\mathcal{M}_1(k;\omega)+\mathcal{M}_2(k;\omega)]\right\}^{-1}_{\omega=e_1(k)} . \tag{2.15}$$

It has recently been suggested[18] that the contribution $M_3(k)$ is almost cancelled by the diagram $M_3^{(p)}$ of Fig. 1. This should be studied further because it was not taken into account that, in the diagram $M_3^{(p)}$, the reaction matrix that connects the lines k and p' is "off-the-energy shell," i.e., that its energy parameter w [Eq. (2.2)] depends on the momenta h', h'', and p'' in addition to k and p', see Eq. (A4) of Ref. 9.

III. MOMENTUM DISTRIBUTION

The correlated ground state contains two-particle–two-hole and more complicated configurations. Therefore, a hole momentum state $h<k_F$ is partly empty, and a particle momentum state $p>k_F$ is partly occupied. The main interest of the resulting momentum distribution is threefold. (i) It enters in analyses of inclusive electron-scattering experiments.[19] (ii) The occupation probability of a shell-model orbit can be obtained from exclusive $(e,e'p)$ experiments;[20] these occupancies are affected by surface effects for weakly bound orbits, but should be comparable to the nuclear matter predictions for deeply bound orbits. (iii) The rate of convergence of the hole-line expansion is governed by the amount of depletion of the Fermi sea.[21]

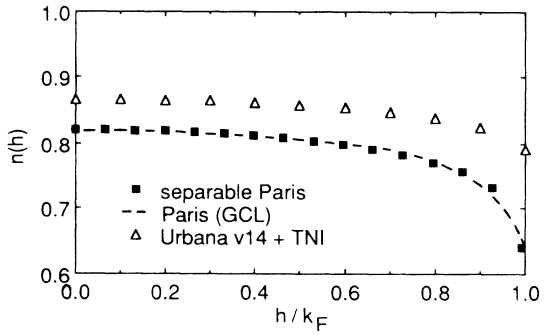

FIG. 4. Momentum distribution below the Fermi surface. The dashed curve (Ref. 15) has been calculated from the original Paris interaction and the solid squares from its separable representation, in both cases for $k_F=1.36$ fm^{-1}. The open triangles have been calculated from the Urbana $v14$ interaction (to which an effective three-body interaction has been added) for $k_F=1.33$ fm^{-1}, in the framework of the correlated-basis perturbation approach. (Ref. 22).

This section is devoted to the calculation of the momentum distribution $n(k)$ up to second order in Brueckner's reaction matrix. It is given by the following expressions ($h,h'<k_F$, $p,p'>k_F$):[13]

$$n_2(h)=1-\tfrac{1}{2}\sum_{h'pp'}\frac{|\langle hh'|g[e_1(h)+e_1(h')]|pp'\rangle|^2}{[e_1(h)+e_1(h')-e_1(p)-e_1(p')]^2}\ , \tag{3.1a}$$

$$n_2(p)=\tfrac{1}{2}\sum_{hh'p'}\frac{|\langle hh'|g[e_1(h)+e_1(h')]|pp'\rangle|^2}{[e_1(h)+e_1(h')-e_1(p)-e_1(p')]^2}\ , \tag{3.1b}$$

They fulfill the same sum rule as the exact momentum distribution $n(k)$, namely

$$\frac{3}{k_F^3}\int_0^\infty n_2(k)k^2dk=1\ . \tag{3.2}$$

A. Momenta smaller than k_F

From Eqs. (2.2), and (2.6a) one readily obtains

$$n_2(h)=\left[1+\frac{\partial}{\partial\omega}\mathcal{M}_1(h;\omega)\right]_{\omega=e_1(h)}\ .$$

In the case of a separable interaction, the ω dependence of $\mathcal{M}_1(k;\omega)$ is algebraic [see Eq. (5) of Ref. 14], so that $n_2(h)$ can be calculated with a very good accuracy. The upper part of Fig. 4 represents the calculated values of $n_2(h)$ for $h<k_F$. It is seen that, in this domain, the momentum distribution mainly depends upon the ratio h/k_F; this is in keeping with findings obtained in the framework of the correlated-basis perturbation expansion.[22] The following parametrization is quite accurate ($h<k_F$, $1.1<k_F<1.75$ fm^{-1}):

$$n_2(h)=0.79-0.13\left[\frac{h}{k_F}\right]-0.19\left[1-\frac{h}{k_F}\right]\ln\left[1-\frac{h}{k_F}\right]\ . \tag{3.3}$$

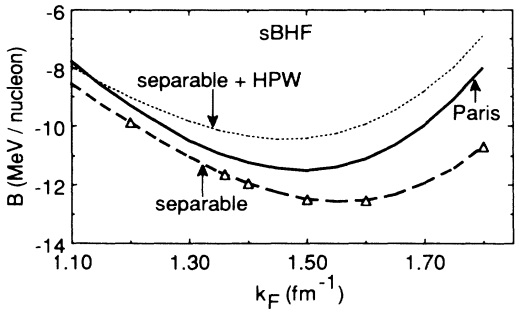

FIG. 5. Average binding energy per nucleon as calculated from the *s*BHF approximation, in which the standard choice is adopted for the auxiliary potential. The solid curve (Ref. 43) has been calculated from the original Paris interaction, and the long-dashed curve from its separable representation of Ref. 5 (upper part of Fig. 12). The dotted curve has been obtained by adding the contribution of the HPW as approximated by Eq. (A1).

In Fig. 4, we compare our result with the one obtained in Ref. 15 from the original Paris interaction; the very good agreement between the two calculations reflects the fact that the 2% difference between the matrix elements of g implied by Fig. 5 entails a difference smaller than 0.01 on the calculated depletion. Figure 4 also shows that the Urbana $v14$ interaction yields a smaller depletion than the Paris interaction; this is possibly due to the fact that the latter contains a stronger tensor component.

As mentioned in connection with Eq. (2.13a), the depletion of the Fermi sea can be characterized by the value $[1-n_2/(h)]$ at the most likely value of h inside the Fermi sea, namely at $h=0.75k_F$:

$$\kappa=[1-n_2(h)]_{h=0.75k_F}\ . \tag{3.4a}$$

Another possible measure of the depletion is provided by the fraction of the nucleons with momenta smaller than k_F, i.e., by the quantity $1-N_<$ with

$$N_<=\frac{3}{k_F^3}\int_0^{k_F}n_2(h)h^2dh\ . \tag{3.4b}$$

Figure 6 shows that the quantities κ and $(1-N_<)$ are close to one another. The depletion of the Fermi sea reaches about 25 per cent in the range of densities considered here. The depletion parameter κ is closely related to the "wound parameter," which is believed to characterize the rate of convergence of the hole-line expansion.[2,21] The plusses in Fig. 6 show the wound parameter that is obtained from the Argonne $v14$ interaction in the framework of the *standard* BHF approximation in which $U(p)$ is set equal to zero for $p>k_F$. It is seen to be quite small; this can be ascribed to the fact that *for the standard choice of* $U(k)$ the two-particle–two-hole configurations all lie at high excitation energies. The solid squares in Fig. 6 show how these results are modified when one adds the contribution of three-hole line and of generalized ring diagrams to the *standard*

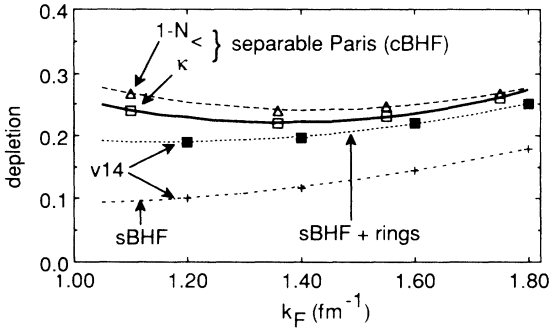

FIG. 6. Dependence upon k_F of the depletion parameter κ [Eq. (3.4a), open squares and thick solid curve] and of $(1-N_<)$ [Eq. (3.4b), open triangles and long-dashed curve] as calculated from the separable representation of the Paris interaction. The other symbols represent the "smallness parameter" of Brueckner's hole line expansion in the case of the Argonne $v14$ interaction: the plusses (dashed-dotted curve) are obtained from the standard BHF approximation, while the solid squares (dotted line) include the contribution of the three-hole line and of "generalized ring" diagrams (Ref. 23).

BHF approximation: The wound parameter then becomes in fair agreement with the momentum distribution represented by the solid squares in Fig. 4. Figure 6 thus supports the claim that it is preferable to adopt a continuous choice for $U(k)$ if one wants to truncate the hole line after its lowest order (BHF) term. Note that in the correlated-basis perturbation expansion one also uses a continuous choice for $U(k)$ for calculating $n(k)$. To the best of our knowledge, no calculation of the momentum distribution $n(k)$ based on the standard choice of $U(k)$ has been published.

B. Momenta larger than k_F

The lower part of Fig. 7 shows that, *in the domain* $0<k/k_F<2$, the momentum distribution primarily depends upon the ratio k/k_F. The dashed curve represents the following parametrization:

$$n_2(p)=0.215+0.3\tan^{-1}x+0.82\ln x\ , \tag{3.5a}$$

where

$$x=(p/k_F-1)/[(p/k_F)^2+1]\ . \tag{3.5b}$$

This expression was suggested by results obtained in the dilute Fermi gas model.[24] It should not be used for larger momenta. Indeed, Fig. 8 shows that, *in the domain* $2<k<4.5\ fm^{-1}$, it should be replaced by the following exponential law (k and k_F in fm^{-1}):

$$n(k)=\frac{k_F^5}{7}\exp(-1.6k)\ . \tag{3.5c}$$

This exponential law is in good agreement with the result found in Ref. 15 for $k_F=1.36$ fm^{-1}. It is also in keeping with calculations made in finite nuclei.[25–28] This is interpreted as an evidence that, in this domain of momenta, the distribution is determined by two-body correlations;[25] this interpretation is confirmed by experimental data on the ^{3}He$(e,e'p)$ and ^{2}H$(e,e'p)$ reactions.[29] The exponential decay is also in keeping with other experimental data surveyed in Ref. 30.

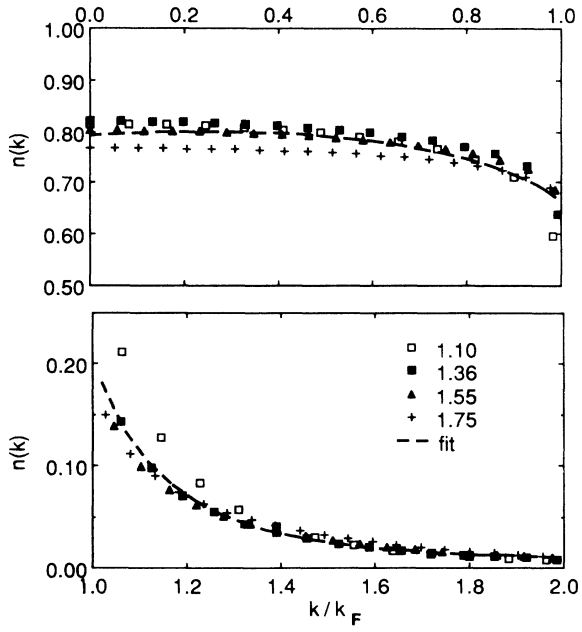

FIG. 7. The symbols show the calculated momentum distribution in the correlated ground state, for the Fermi momenta $k_F=1.10$ fm^{-1} (open squares), 1.36 fm^{-1} (solid squares), 1.55 fm^{-1} (solid triangles), and 1.75 fm^{-1} (plusses). The dashed curves represent the parametrizations (3.3) and (3.5a).

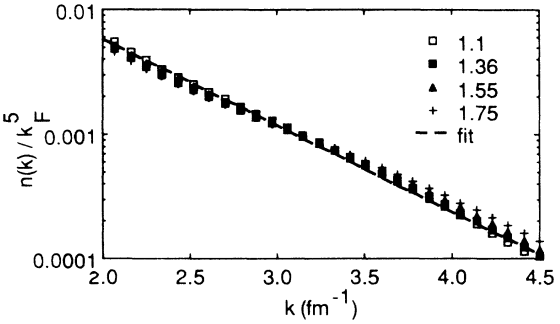

FIG. 8. The symbols give the calculated values of $n(k)/k_F^5$, for the Fermi momenta 1.10, 1.36, 1.55, and 1.75 fm^{-1}; the notation is the same as in Fig. 3. The dashed line represents the exponential parametrization (3.5c)

For very large values of p, the momentum distribution $n(p)$ is expected to decrease as an inverse power law.[25,31] For a Yukawa interaction, for instance, $n(p)$ decreases as p^{-8} for very large p, where it is moreover proportional to k_F^6: this can be checked analytically from Eq. (3.1b).

In Ref. 15, the momentum distribution $n(k)$ has been calculated up to $k=2.8$ fm^{-1}, for $k_F=1.36$ fm^{-1} and using as input the original Paris interaction. We showed in Fig. 4 that these results are in very good agreement with ours for $k<k_F$. This also holds true up to $k=2.8$ fm^{-1}; this is illustrated by the fact that the contribution of the interval (0, 2.8 fm^{-1}) to the left-hand side of the sum rule (3.2) was found equal to 0.96 in Ref. 15, which is quite close to the value of 0.98 obtained from our results. It should be realized that this does not imply that the calculations are very accurate. Indeed, the left-hand side of Eq. (3.2) is equal to 1.04 when the integration is carried out up to 4.5 fm^{-1} ($k_F=1.36$ fm^{-1}). A crude extrapolation of the range of integration towards infinity shows that the left-hand side of Eq. (3.2) may be as large as 1.09, in the case $k_F=1.36$ fm^{-1}. We believe that this overshoot of the sum rule (2.2) is mainly due to the use of an angle-average expression in the summation over h and h' on the right-hand side of Eq. (3.1b). This approximation was used here as well as in Ref. 15. An angle average was also used for evaluating the sum over p,p' on the right-hand side of Eq. (3.1a), but this is the same as that involved in the calculation of the reaction matrix [Eq. (2.2)] and is known to be accurate.[32] Hence, we believe that the calculated $n_2(k)$ is more accurate for $k<k_F$ than for $k>k_F$.

C. Quasiparticle strength

The quasiparticle strength is defined by Eq. (2.10). Its value at the Fermi momentum is equal to the difference

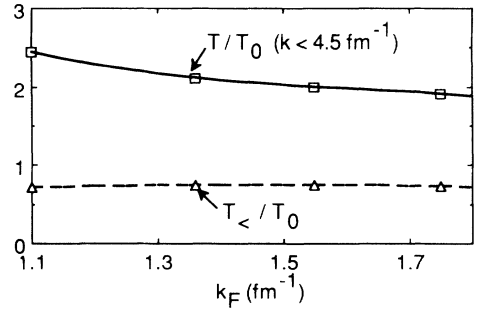

FIG. 9. The solid curve (squares) represents the average kinetic energy per nucleon of the correlated ground state divided by that of the uncorrelated ground state. The dashed curve (triangles) gives the value of this ratio when one only includes the nucleons with momentum smaller than k_F. The symbols are the values that have actually been calculated [with a cutoff at 4.5 fm^{-1} in the integral over particle momenta on the right-hand side of Eq. (4.1a)], while the curves are fits.

between the occupation probabilities right below and right above k_F:[33]

$$Z(k_F)=n(k_F-0)-n(k_F+0) . \tag{3.6}$$

Figure 3 represents the value of $Z(k_F)$ derived from the momentum distribution calculated. In nuclei, the quasiparticle strength is expected to be larger than in nuclear matter because an energy gap separates the two valence shells. At $k_F=1.36$ fm^{-1}, our result (0.44) is in good agreement with that (0.47) found in Ref. 15. The smallness of $Z(k_F)$ illustrates our previous warning that $M_1(k)+M_2(k)$ should not be identified with the second-order approximation to the potential energy [Eq.(2.9b)].

IV. AVERAGE KINETIC ENERGY PER NUCLEON

The average kinetic energy per nucleon is given by

$$T=\frac{3}{k_F^3}\int_0^\infty n(k)\frac{k^4}{2m}dk . \tag{4.1a}$$

In the unperturbed ground state, this quantity is equal to $T_0=0.3k_F^2/m$. When ground-state correlations are taken into account, T becomes larger than T_0 since part of the nucleons have then momenta larger than k_F. The calculated values of T/T_0 are represented by the solid curve in Fig. 9. There, the dashed curve shows the ratio $T_<\,/T_0$, where

$$T_<=\frac{3}{k_F^3}\int_0^{k_F} n(k)\frac{k^4}{2m}dk \tag{4.1b}$$

is the contribution of the nucleons that lie below the Fermi surface. The ratio $T_<\,/T_0$ is nearly independent of k_F, in keeping with the near constancy of $N_<$ (Fig. 6). The ratio T/T_0 is close to 2 for all k_F. Note, however, that the calculated T/T_0 are underestimates since our calculation of $n(p)$ extends only up to $p=4.5$ fm^{-1}; a crude extrapolation of $n(p)$ towards very large p suggests that T/T_0 may be as large as 3 for $k_F=1.36$ fm^{-1}, instead of the value 2.1 shown in Fig. 9. This illustrates that caution must be exercised in theoretical approaches in which the average binding energy per nucleon is written as the sum of the average kinetic energy and of the average interaction energy. The size of the contribution of large momenta to T reflects the slowness of the decrease of $[p^4n(p)]$ for large p; this property may be a special feature because of the momentum dependence of the Paris interaction.

V. MEAN-SQUARE DEVIATION FROM THE UNPERTURBED FERMI SEA

Let $\rho(\mathbf{r},\mathbf{r}')$ denote the one-body density matrix of a finite nucleus with A nucleons and $\rho_0(\mathbf{r},\mathbf{r}')$ be its value associated for the uncorrelated system. The quantity

$$\sigma=A^{-1}\mathrm{trace}(\rho-\rho_0)^2 \tag{5.1a}$$

characterizes the deviation of ρ_0 from ρ. Note that σ involves diagonal and off-diagonal elements of ρ; in particular, it involves both the density and the momentum distribution. The value of σ depends upon the choice of single-particle orbitals. It is minimum when the latter are the natural orbitals obtained by diagonalizing ρ. The existence of this minimum indicates that one cannot very accurately approximate both the density and the momentum distributions from a Slater determinant, or equivalently reflects the limitation of any static mean-field approximation, like for instance the Hartree-Fock approximation.[34]

Nuclear matter presents the advantage that the natural orbitals are known (plane waves). The expression of σ then takes the simple following form:[35]

$$\sigma=\sigma_<+\sigma_> , \tag{5.1b}$$

where

$$\sigma_<=\frac{3}{k_F^3}\int_0^{k_F}[1-n(h)]^2h^2dh , \tag{5.1c}$$

$$\sigma_>=\frac{3}{k_F^3}\int_{k_F}^{\infty}[n(p)]^2p^2dp . \tag{5.1d}$$

Figure 10 represents the values of $\sigma_<$, $\sigma_>$, and σ as com-

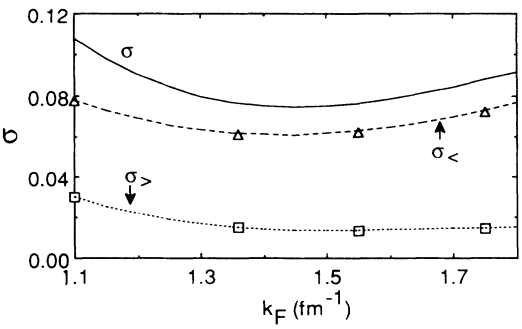

FIG. 10. The solid curve represents the mean-square deviation σ [Eq. (5.1)]. The long-dashed curve corresponds to $\sigma_<$ [Eq. (5.1b)] and the short-dashed line to $\sigma_>$ [Eq. (5.1c)].

puted from the momentum distributions calculated in Sec. III. Our calculated values of $\sigma_<$ are larger than the largest value (≈ 0.03) considered in the models constructed in Ref. 35 for the correlated ground state of ^{208}Pb. This reflects the largeness of the depletion of the Fermi sea. Relatedly, our calculated values of $\sigma_>$ are much larger than the largest value (≈ 0.04) considered in the models of Ref. 35; this is also due to the fact that our calculation includes momenta up to 4.5 fm^{-1} [the corresponding $e(p) \approx 440$ MeV], while in Ref. 35 the occupation probability was set equal to zero for orbits with energy larger than 120 MeV.

VI. AVERAGE BINDING ENERGY PER NUCLEON

The full Hamiltonian H is written in the form

$$H = (\mathcal{T} + U) + (\mathcal{V} - U) , \tag{6.1}$$

where $\mathcal{T}$ is the kinetic energy operator, $\mathcal{V}$ is the sum of the two-body interactions and U is the auxiliary one-body potential of Eq. (2.1). In Brueckner's approach, the average binding energy per nucleon (in short binding energy) is written as the sum of the kinetic energy T_0 of the unperturbed Fermi sea and of a correction D:

$$B = T_0 + D . \tag{6.2}$$

In this section, we shall calculate the contributions to D that are represented by the diagrams of Fig. 11. We shall also discuss the relationship between the Brueckner and the Green's function approaches. In Secs. VI A and VI B, we identify the auxiliary potential with the BHF

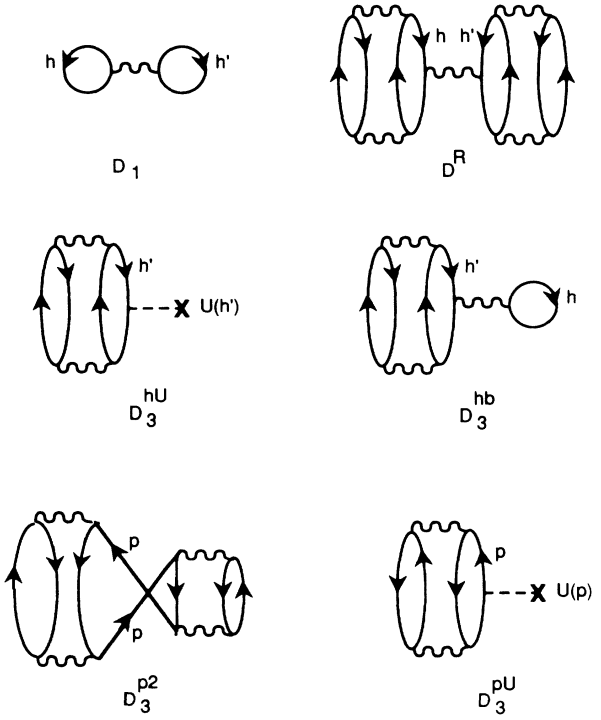

FIG. 11. Diagrammatic representation of several contributions to the hole-line expansion of the average binding energy per nucleon that are calculated in Sec. VI.

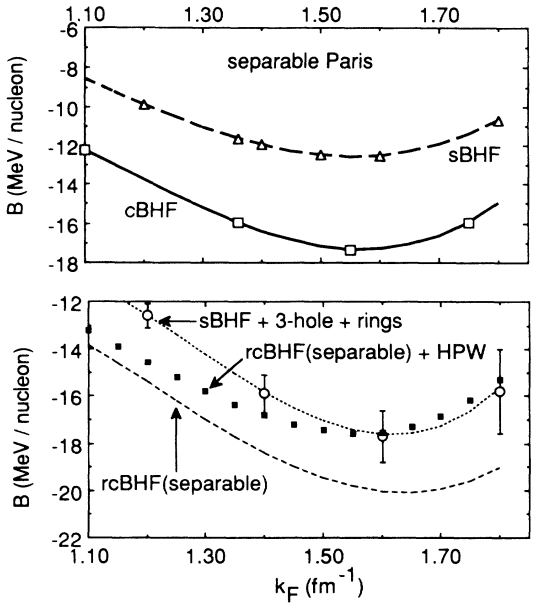

FIG. 12. Average binding energy per nucleon versus the Fermi momentum. In the upper drawing, the solid curve (squares) corresponds to the *c*BHF approximation [$U(k) = M_1(k)$ for all k], and the long-dashed line (triangles) to the *s*BHF approximation [$U(k) = M_1(k)$ for $k < k_F$, $U(k) = 0$ for $k > k_F$]; in both cases the input is the separable representation of the Paris interaction. In the lower drawing, the long-dashed line represents the renormalized *c*BHF (*rc*BHF) approximation as calculated from the separable representation of the Paris interaction; the solid squares have been obtained by adding to this *rc*BHF approximation an estimate [Eq. (A1)] of the contribution of the high partials waves (HPW) omitted in the separable approximation; the open circles and attached error bars are taken from Ref. 23: They have been calculated from the original Paris interaction and include the sum of the *s*BHF approximation and of the three-hole line and of the "generalized ring" diagrams.

potential energy for all values of k, [Eq. (2.4a)]; we shall specify this by a label c, where c refers to "continuous." For instance, *c*BHF is the BHF approximation with the continuous choice $U(k) = M_1(k)$ for all k. Likewise, *s*BHF denotes the BHF approximation for the "standard" choice in which $U(k) = M_1(k)$ for $k < k_F$ and $U(k) = 0$ for $k > k_F$ (see the Appendix).

A. BHF approximation

The BHF approximation to D is represented by the diagram labeled D_1 in Fig. 11; its expression reads

$$D_1 = \tfrac{1}{2} \sum_{hh'} \langle hh' | g [e(h) + e(h')] | hh' \rangle = \tfrac{1}{2} \sum_h M_1(h) , \tag{6.3}$$

where $M_1(h)$ is defined by Eqs. (2.3). The corresponding value of the binding energy depends upon the choice of $U(k)$. In the upper part of Fig. 12, the solid curve corresponds to the *c*BHF and the long-dashed line to the *s*BHF approximation. The continuous choice yields binding energies that are sizably larger than in the stan-

dard choice. This is a desirable feature. Indeed, there exists strong evidence that the *s*BHF approximation to the binding energy lies above an upper bound evaluated in the framework of the hypernetted chain expansion;[21,23] this is interpreted as indicating that the higher order corrections to the BHF approximation are sizable when the standard choice is adopted.[7,36,37]

B. Renormalization correction

The diagrams D^R, D_3^{hU}, and D_3^{hb} of Fig. 11 have the following physical interpretation. The BHF approximation does not take into account the fact that the hole momentum states h and h' are partly empty. It thus appears natural to replace D_1 by the following "renormalized" expression:

$$D_1^R=\tfrac{1}{2}\sum_{hh'} n(h)n(h')\langle hh'|g[e(h)+e(h')|hh'\rangle \ , \tag{6.4}$$

where $n(h)$ is the occupation probability of the hole momentum state h. Using $n(h)\approx 1-\kappa_2(h)$, where $\kappa_2(h)$ is the second-order approximation (2.12a), one finds

$$D_1^R=D_1+D^R+D_3^{hb} \ . \tag{6.5}$$

If the auxiliary potential $U(k)$ is chosen equal to the BHF potential $M_1(k)$ for $k<k_F$, the last term on the right-hand side of Eq. (6.5) is cancelled by D_3^{hU}:

$$D_3^{hU}\ D_3^{hb}=0 \quad \text{for } U(h)=M_1(h) \ . \tag{6.6}$$

Equations (6.5) and (6.6) yield

$$D_1^R+D_3^{hU}=D_1+D^R \ . \tag{6.7}$$

The approximation $D^R\approx\kappa^2 D_1$ is quite accurate. The "renormalized BHF approximation" to the binding energy thus reads

$$B_1^R\approx T_0+(1+\kappa^2)D_1 \ . \tag{6.8}$$

This renormalized BHF approximation is represented by the long-dashed curve in the lower part of Fig. 12. Our results have been derived from a separable representation of the original Paris interaction. In the Appendix we recall that this separable representation omits the contribution of high partial waves (HPW). The solid squares in the lower part of Fig. 12 represent the sum of B_1^R and of the crude estimate of the contribution of the HPW given in the Appendix.

Day and Wiringa[23] used the original Paris interaction as input, adopted the standard choice for the auxiliary potential, and added the *s*BHF, three-hole line and "ring diagrams" contributions. Their results are represented by the open circles in the lower part of Fig. 12, with attached estimated uncertainties; they are seen to be fairly close to those obtained from the renormalized BHF approximation when one adopts the continuous choice for the auxiliary potential and includes the contribution of HPW. This supports the claim[7,36] that the size of the corrections to the BHF approximation is reduced if one adopts the continuous rather than the standard choice for the auxiliary potential. This is of practical importance since these corrections are very difficult to evaluate.

C. Mass operator as an auxiliary potential

Analytical arguments exist for choosing the auxiliary potential $U(k)$ equal to the full mass operator $M(k)$ rather than to its BHF approximation, especially for k in the vicinity of k_F.[7,9,10,13,37–39] Recently, calculations of the binding energy have been performed in which $U(k)$ is taken equal to the sum $M_1(k)+M_2(k)$ [Eq. (2.5)].[14] We place a tilde over the corresponding quantities, e.g.,

$$\tilde{U}(k)=M_1(k)+M_2(k) \ . \tag{6.9}$$

Figure 2 shows that $M_2(k)$ decreases the average energy difference between particles and hole states; hence, it leads to an increase of the binding energy. This is confirmed by the comparison between the solid curve and the long-dashed line in Fig. 13. One must keep in mind that when $U(h)$ differs from $M_2(h)$ the diagrams D_3^{hU} and D_3^{hb} of Fig. 11 do not cancel each other. It therefore appears more consistent to consider the variation of the sum $T_0+D_1+D_3^{hU}+D_3^{hb}$. This sum is equal to B_1 when $U(k)=M_1(k)$; when $U(k)$ is chosen equal to $M_1(k)+M_2(l)$, the value of this sum is represented by the short-dashed curve in Fig. 13. It is seen to be fairly close to the solid curve, i.e., to the *c*BHF approximation B_1 considered in the previous sections. One should moreover take into account that when $U(k)$ is taken equal to $M_1(k)+M_2(k)$ rather than to $M_1(k)$, this modifies the value of the diagram D_3^{pU} of Fig. 11 by a quantity $D_3^{pM_2}$. The quantity

$$\tilde{\mathcal{B}}=\tilde{B}_1+D_3^{hU}+D_3^{hb}+D_3^{pM_2} \ , \tag{6.10}$$

is represented by the dots in Fig. 13; it is almost equal to B_1 [to which it would reduce if one would set $U(k)=M_1(k)$]. The property that the right-hand side of Eq. (6.10) is fairly insensitive to modifications of $U(k)$ had been conjectured in Ref. 40. Note that the property $\tilde{\mathcal{B}}\approx B_1$ does not imply that this quantity is an accurate approximation to the actual binding energy; for instance, the term $D_3^{pM_2}$ on the right-hand side of Eq. (6.10) is cancelled by the diagram D_3^{p2} of Fig. 11 [see Eq. (6.11)].

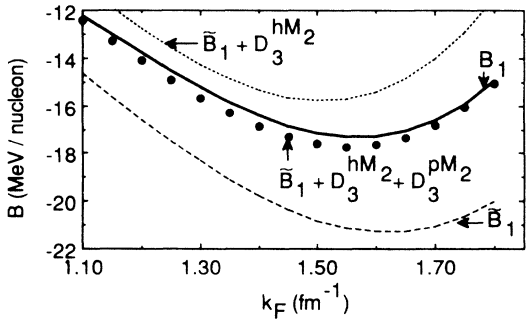

FIG. 13. Average binding energy per nucleon. The BHF approximation is represented by the solid curve when $U(k)=M_1(k)$, and by the long-dashed curve when $U(k)=M_1(k)+M_2(k)$ (Ref. 14). The short-dashed curve gives the sum of the diagrams $\tilde{B}_1$, D_3^{hU}, and D_3^{hb} of Fig. 10. The dots represent the sum $\tilde{\mathcal{B}}=\tilde{B}_1+D_3^{hM_2}+D_3^{pM_2}$.

D. Potential insertions on particle lines

If $U(k)\neq 0$ for $k > k_F$, the diagram D_3^{pU} of Fig. 11 exists and is not negligible. For instance, we evaluated $D_3^{pM_2}$ in the previous section and found that its magnitude is about -1 to -3 MeV in the considered range of Fermi momenta. One should, however, keep in mind that the magnitude of the graph obtained by adding a U insertion to an original diagram is comparable to that of a graph obtained by adding one hole line to the original diagram. This is illustrated by the property (6.6) as well as by the following:

$$D_3^{p2}+D_3^{pM_2}=0 \ . \tag{6.11}$$

The latter relation is at the origin of the choice $U(p)=M_2(p)$ for $p > k_F$ advocated by Brandow.[31] Since $M_2(k)$ is small for $k > k_F$, it is more convenient to set $U(k)$ equal to zero for $k=0$ and to evaluate the diagram D_3^{p2} explicitly: This is the "standard choice."

In this paper we have taken $U(k)=M_1(k)$ for all k. Then, a contribution $D_3^{pM_1}$ exists. Figure 14 shows that the diagram $D_3^{pM_1}$ is quite large. Therefore, the continuous choice $U(k)=M_1(k)$ can be successful only if the diagram $D_3^{pM_1}$ is approximately cancelled by the sum of all the three-hole line diagrams. It was argued in Ref. 13 that this may indeed be the case. However, the size of $D_3^{pM_1}$ should remind us that a reliable evaluation of the binding energy necessitates the investigation of the sum of the three-hole line diagrams. This has not yet been performed in the case of the continuous choice.

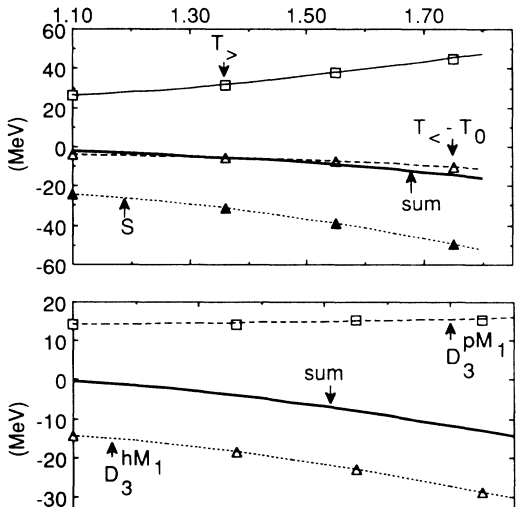

FIG. 14. The upper drawing gives the values of graphs that appear in the hole-line expansion based on the Green's function approach, see the left-hand side of Eq. (6.16): The open squares (thin solid line) represent $T_>$, the open triangles (long-dashed curve) $T_< - T_0$, the solid triangles (dotted line) S and the thick solid curve the sum of these three contributions. The lower drawing shows the values of diagrams that appear in the Brueckner hole line expansion, see the right-hand side of Eq. (6.16): The open squares (long dashed line) represent $D_3^{pM_1}$, the open triangles $D_3^{hM_1}$ and the solid curve the sum of these two contributions. The continuous choice (2.4a) has been adopted for $U(k)$.

E. Comparison with the Green's function approach

Let Ψ_0 denote the wave function of the correlated ground state and ϕ_0 that of the uncorrelated ground state. In the Brueckner approach, one writes the ground-state energy in the form

$$\mathcal{B}=\langle\phi_0|(\mathcal{T}+U)+(\mathcal{V}-U)|\Psi_0\rangle/\langle\phi_0|\Psi_0\rangle \ . \tag{6.12}$$

In the Green's function approach, one rather starts from

$$\mathcal{B}=\langle\Psi_0|(\mathcal{T}+U)+(\mathcal{V}-U)|\Psi_0\rangle/\langle\Psi_0|\Psi_0\rangle \ . \tag{6.13}$$

In both cases, one performs a linked cluster expansion of $\Psi_0/\langle\phi_0|\Psi_0\rangle$ or of $\Psi_0/\langle\Psi_0|\Psi_0\rangle$. It is apparent from Eq. (6.13) that in the Green's function approach this amounts to expand separately the expectation value of the kinetic and of the interaction energy, while in the Brueckner approach this leads to an expansion of the type (6.2). The Brueckner approach is the one that is most often used in studies of the binding energy; however, it is not well suited for the analysis of other quantities. In contrast, a starting point of type (6.13) is most natural for evaluating the expectation value of quantities other than the Hamiltonian, e.g., the one-body Green's function, the mass operator, the spectral function, the momentum distribution, etc. In the case of the expansion of the binding energy, the relationship between the two approaches has been investigated in Ref. 11; we are now in a position to provide numerical values for some of the relevant quantities.

Let us write the binding energy in the form

$$B=T_0+D_1+C \ , \tag{6.14}$$

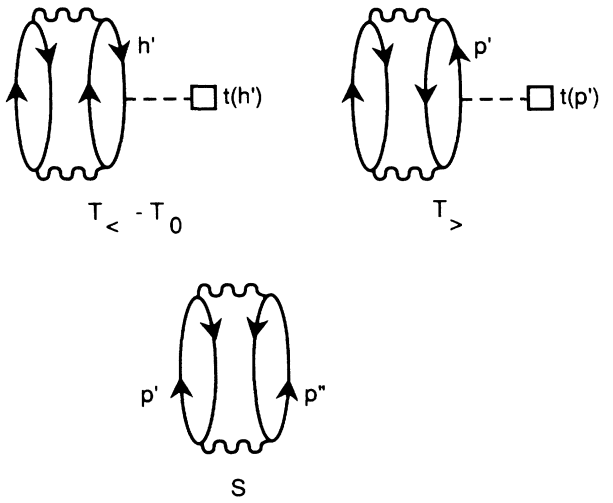

FIG. 15. Second-order contributions to the quantity C that appears in the Green's function expansion [Eq. (6.14)]. A square represents the kinetic energy operator, e.g., $t(k)=k^2/2m$.

where C is the correction to the BHF approximation. In the Green's function approach, one finds that, up to second order in the reaction matrix, C is the sum of the diagrams shown in Fig. 15.[11] There, the graph $T_>$ represents the lowest-order contribution of the nucleons with momenta $p > k_F$ to the kinetic energy T, namely

$$T=\frac{3}{k_F^3}\int_{k_F}^{\infty} n_2(p)\frac{p^4}{2m}dp \ . \tag{6.15}$$

The upper left diagram is the quantity $T_< - T_0$, i.e., the correction to the kinetic energy T_0 of the uncorrelated system that is due to the nucleons with momenta smaller than k_F [Eq. (4.1b)]. The diagram S of Fig. 15 involves two consecutive reaction matrices in a particle-particle ladder. This type of diagram does not appear in the Brueckner-type expansion. Its occurrence in the Green's function approach was clarified in Ref. 11, where the following identity was proved:

$$(T_< - T_0)+T_> +S = D_3^{hU}+D_3^{pU} \ ; \tag{6.16}$$

the right-hand side refers to diagrams of Fig. 11. We emphasize that the identity (6.16) holds regardless of the specific choice made for $U(k)$. In Fig. 14, we give the values of the various quantities which appear in Eq. (6.16), for the continuous choice (2.4a). It is seen that most of these quantities are quite large compared to the left- or right-hand side of Eq. (6.16)]. This illustrates the importance of grouping terms that have comparable absolute magnitudes but opposite signs. Incidentally, very large values of p' influence the calculated values of $T_>$ and S; since we do not include values of $p' > 4.5$ fm^{-1}, the identity (6.16) is only approximately fulfilled.

VII. THE HUGENHOLTZ-VAN HOVE THEOREM

The Hugenholtz-Van Hove theorem[12] states, in particular, that at equilibrium the average binding energy per nucleon is equal to the Fermi energy, i.e., to the energy of a quasiparticle with momentum k_F. The degree of fulfillment of the Hugenholtz-Van Hove theorem indicates to what extent the various approximations are consistent. We consider the continuous choice for the auxiliary potential, Eq. (2.4a). The corresponding BHF approximation to the binding energy is represented by the solid curve in Fig. 15. The BHF approximation to the mass operator is given by $M_1(k_F)$ and the corresponding Fermi energy by

$$E_F^{(1)}=k_F^2/2m+M_1(k_F) \ . \tag{7.1}$$

This quantity is represented by the short-dashed curve in Fig. 16. It is seen that the Hugenholtz-Van Hove theorem is badly violated. The origin of this failure has been discussed by Brueckner and Goldman,[16] whose argument we now adapt to this context.

Let us write the BHF approximation to the binding energy in the form

$$B_1=T_0+D_1+D_3^{hU}+D_3^{hb} \ . \tag{7.2}$$

The removal energy of a nucleon with momentum h is given by the functional derivative of B_1 with respect to the corresponding occupation number in the Fermi momentum distribution. The functional derivative of D_1 is $M_1(h)+M_2(h)$, where the occurrence of M_2 is due to the numerator in the second term on the right-hand side of Eq. (2.2). The authors of Ref. 16 also took the functional derivative of the energy denominator on the right-hand side of Eq. (2.2). It is more convenient to consider that the auxiliary potential $U(h)$ is fixed, and thus independent of the occupation number. Then, the functional derivative of $D_3^{hU}+D_3^{hb}$ is given by M_3 (see Fig. 1). Complications arise because the mass operator is frequency dependent; a reasoning similar to the one that led to Eq. (2.14) yields the following expression for the Fermi energy when the contributions of M_1, M_2, and M_3 are taken into account:

$$E_F^{(1+2+3)}\approx k_F^2/2m+[1-\kappa Z]M_1(k_F)+Z(1-\kappa)M_2(k_F) \ , \tag{7.3}$$

where Z is the quasiparticle strength previously plotted in Fig. 3. The approximation (7.3) for the Fermi energy is represented by the long dashed curve in Fig. 16. It intersects the solid curve close to the saturation point. The Hugenholtz-Van Hove theorem is thus quite well fulfilled if one uses the BHF approximation for the binding energy and a suitably adapted approximation for the mean field. Note that the latter "adapted" approximation is not the BHF approximation.

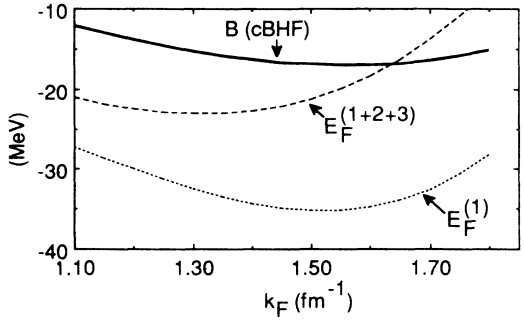

FIG. 16. The solid curve represents the BHF approximation to the average binding energy per nucleon for the continuous choice of $U(k)$, see the upper part of Fig. 12. The short-dashed curve gives the Fermi energy as evaluated from the BHF approximation to the mass operator [Eq. (7.1)]. The long-dashed curve represents the approximation (7.3) for the Fermi energy.

VIII. SUMMARY AND CONCLUSION

Nuclear matter is a hypothetical medium. It nevertheless plays an important role because its uniform nature considerably simplifies the calculations, and because some of its properties can be compared with "empirical values" deduced from extrapolations of observed nuclear data towards large mass numbers. Among these properties, the following ones have been investigated in the present paper: (i) the average binding energy per nucleon; (ii) the average potential energy of a nucleon as a function of the nucleon momentum; (iii) the Fermi energy

(iv) the occupation probability of single-particle orbits. We also discussed properties whose interest is more theoretical than empirical, namely; (v) the average kinetic energy per nucleon in the correlated system; (vi) the mean-square deviation of the one-body density matrix from that of the unperturbed Fermi sea; (vii) the strength of a quasiparticle located at the Fermi sea.

All these properties can be derived from the one-body Green's function or equivalently from the mass operator. The latter would therefore be expected to play a central role in studies of nuclear matter. This is, however, not the case in most papers because these only deal with the average binding energy. For that purpose, they use the Bethe-Brueckner hole-line expansion, whose starting point is Eq. (6.12). We rather use a Green's function approach, based on Eq. (6.13). In the Green's function as well as in the Bethe-Brueckner approach one adds to and subtracts from the Hamiltonian an auxiliary one-body potential $U(k)$ [Eq. (6.1)], and one then performs a linked cluster expansion in either Eq. (6.12) or Eq. (6.13). In practical applications the expansion has to be truncated; this is why the calculated result depends upon the choice of the auxiliary potential.

In the Bethe-Brueckner approach to the binding energy it is considered that the "best" choice of the auxiliary potential is the one that optimizes the convergence of the linked cluster expansion; it was generally believed that this criterion is nearly fulfilled by the "standard choice" in which $U(k)$ is set equal to zero for k larger than the Fermi momentum k_F, and is large and negative for $k<k_F$. This standard choice is numerically quite convenient; furthermore, those corrections to the corresponding BHF approximation which have been evaluated are not very large.[21] The possibility should nevertheless be kept in mind that this standard hole-line expansion might not converge towards the correct answer.[42] Moreover, the corrections to the standard BHF approximation are not sufficiently small to be neglected; this complicates the construction of an effective nucleon-nucleon interaction.[8] Finally, the standard choice appears inappropriate when properties other than the binding energy are considered. For instance, the corresponding momentum distribution does not have a vertical slope at the Fermi surface as it should; this failure persists when one goes beyond the BHF approximation. It is thus not surprising that the standard choice seems awkward when one adopts the Green's function approach,[7,9,10,13,37–39] although the hole-line expansions of the binding energy in the Green's function and Bethe-Brueckner approaches are intimately related.[11]

This is why we chose an auxiliary potential $U(k)$, which is a continuous function of k. In order to simplify the calculation of corrections to the BHF approximation, we use as input a separable representation of the original Paris nucleon-nucleon interaction: The corresponding reaction matrix can be computed rapidly and accurately. We argued in the Appendix (see also Fig. 5) that this separable approximation is faithful, although the contribution of the omitted high partial waves (HPW) is not negligible. The simplest continuous choice consists in identifying $U(k)$ with the BHF approximation to the nucleon potential energy for all values of k, larger as well as smaller than k_F (dots in Fig. 2). The corresponding continuous BHF approximation to the average binding energy is more attractive than the standard BHF approximation (upper part of Fig. 12). When the renormalization diagram D^R of Fig. 11 is included (as well as an estimate of the HPW contribution) one obtains a binding energy (squares in the lower part of Fig. 12), which is quite close to that obtained by adding the BHF, three-hole line and ring diagrams in the standard expansion (dotted curve in the lower part of Fig. 12). This is of practical interest since the renormalized continuous BHF approximation readily lends itself to the construction of an effective interaction and since the continuous choice enables a consistent evaluation of other quantities than the binding energy. In particular, the Fermi energy can be calculated; it nicely fulfills the Hugenholtz-Van Hove theorem (Fig. 16).

According to the analytical arguments of Ref. 7, 9, 10, 13 and 37–39, it would be more consistent to identify the auxiliary potential with the mass operator. When one takes $U(k)=M_1(k)+M_2(k)$ instead of $U(k)=M_1(k)$, the BHF approximation to the binding energy is sizably modified (curve $\tilde{B}_1$ in Fig. 13); however, one recovers a result close to the original one if the modifications of the diagrams D_3^{hU} and D_3^{pU} of Fig. 11 are taken into account (dots in Fig. 13). This indicates that the nice features of the simplest continuous BHF approximation are preserved if one adopts a more sophisticated choice for $U(k)$. Note that these features do not necessarily imply that the calculated binding energy is an accurate approximation of the actual binding energy. This warning is illustrated by the fact that the value of the diagram $D_3^{pM_1}$ is quite large (Fig. 14). The conjecture[7,36,37] that this diagram is approximately canceled by the sum of the three-hole line has not yet been checked numerically. One should also keep in mind the recent claim[43] that the sum of some ring diagrams may be sizable, see however Refs. 44.

The rate of convergence of the hole-line expansion is believed to be determined by the parameter κ, which measures the depletion of the Fermi sea, i.e., the probability that a nucleon has a momentum larger than the Fermi momentum. With the standard choice of $U(k)$, the depletion parameter is quite small when evaluated in the lowest-order approximation (crosses in Fig. 6). This made many believe that the convergence of the standard hole-line expansion is rather fast. However, the inclusion of the three-hole line and of the generalized ring contributions sizably increases the calculated depletion (solid squares in Fig. 6). This reflects the fact that the standard choice artificially suppresses the admixture of two-particle–two-hole configurations in the correlated ground state, because it introduces a large gap between the particle and hole energies. Hence, the smallness of the value of κ calculated from the standard BHF approximation is deceptive. It is also worrisome in view of the claim[45] that the hole-line expansion is useful only if this approximate (BHF) κ is close to the actual depletion. The continuous choice leads to a BHF value of the depletion parameter (open squares in Fig. 6) which is larger than that obtained

from the standard choice.[13] This larger value is close to the one obtained when the contributions of the three-hole line and of the ring diagrams are included in the standard expansion. Hence, it is probably more realistic; this is confirmed by the comparison with results obtained from the correlated basis function approach (open triangles in Fig. 4). The size of κ suggests that the rate of convergence of the hole-line expansion is rather weak for the continuous as well as for the standard choice of $U(k)$, although this is somewhat hidden in the latter case.

If one adopts the Green's function approach, one separately expands the average kinetic energy and the average interaction energy. Thus, new diagrams appear in the expansion of the binding energy (Fig. 15). We have calculated the value of these new graphs and found that most of them are quite large (Fig. 14). This should not be viewed as a drawback of the Green's function approach since the diagrams of Fig. 15 can be combined with other diagrams to recover those of the Brueckner expansion [Eq. (6.16)]. At the same time, the largeness of the average kinetic energy (Fig. 9) indicates that particular caution must be exercised in approaches in which the kinetic energy has to be evaluated.

The momentum distribution below the Fermi surface is of physical interest because recent experimental data on pickup and knockout reactions yield information on the occupation probabilities of shell-model orbits.[20,46,47] In the case of weakly bound orbits, these probabilities are sensitive to nuclear surface effects; however, they should be comparable to nuclear matter values for deeply bound orbits. The momentum distribution for large nucleon momenta is also of interest for the interpretation of inclusive electron scattering data[48] and of the EMC effect.[19] Despite this manifold interest, there exist only very few calculations of the momentum distribution $n(k)$ in nuclear matter, in part because the standard choice of $U(k)$ is not appropriate to study it. We performed a calculation of $n(k)$ with the BHF continuous choice, up to second order in the reaction matrix. The results are shown in Figs. 4, 7, and 8, together with simple parametrizations. For $0<k<2k_F$, the calculated $n(k)$ mainly depends upon the ratio k/k_F, in agreement with results obtained from the correlated basis function approach;[22] our results are in very good agreement with those obtained[15] for $k_F=1.36$ fm^{-1} from the original Paris interaction, which confirms the faithfulness of the separable representation. For $2<k<4.5$ fm^{-1} the calculated $n(k)$ decreases exponentially with increasing k and is proportional to k_F^5 (Fig. 8). For still larger values of k, $n(k)$ is expected to decrease like k^{-8} and to be proportional to k_F^6.

The existence of ground-state correlations imply that it is impossible to exactly reproduce the one-body density matrix of a nucleus if one approximates the ground-state wave function by a Slater determinant. Hence, a Hartree-Fock approximation cannot simultaneously reproduce both the radial density and the momentum distribution. This limitation is characterized by the existence of a minimum value for the mean square deviation from the one-body density matrix. This minimum can be calculated in the case of nuclear matter because the natural orbitals are then known to be plane waves (Fig. 10).

The discontinuity of the momentum distribution at the Fermi surface is equal to the quasiparticle strength of a nucleon with momentum k_F (Fig. 3). In the case of nuclei, this strength can be identified with the "absolute" spectroscopic factor, on which empirical information is becoming available via $(e,e'p)$ reactions;[20,47] the same quantity enters in the analysis of some electron elastic[49] and inelastic scattering data.[50] These data yield a strength that is larger (≈ 0.7) than the value found in nuclear matter. This is expected since in nuclei the value of Z is increased because of the energy gap between the hole and particle valence orbits; in addition, higher-order corrections are likely to increase the calculated value of Z in nuclear matter.[51]

APPENDIX

The calculations reported in this paper use as input a separable representation[5] of the original[6] Paris nucleon-nucleon interaction. When comparing with previous calculations based on the original Paris potential, one should remember that the latter contains many partial waves, while the separable representation only involves the channels $^1S_0$, $^3S_1$-$^3D_1$, $^1P_1$, $^3P_0$, $^3P_1$, $^1D_2$, $^3D_2$, and $^3P_2$-$^3F_2$. In order to estimate the effect of the higher partial waves (HPW), we consider the standard BHF (*s*BHF) approximation, i.e., that associated with the standard choice of the auxiliary potential. Figure 5 shows that the corresponding binding energy as calculated from the separable representation is somewhat lower than that calculated[43] from the original Paris interaction. We now argue that this difference can be ascribed to the HPW. The contribution of the latter is roughly proportional to k_F^3.[52] From the numerical values given by Kuo *et al.*[43] at $k_F=1.4$ and 1.5 fm^{-1}, we obtain the following crude estimate for the contribution of the HPW to the binding energy:

$$B_{\rm HPW} \approx -0.33+0.7k_F^3 \ ; \tag{A1}$$

this parametrization is expected to be approximately valid in the range of values of k_F considered here. By adding it to the *s*BHF approximation derived from the separable interaction one obtains the short dashed curve in Fig. 5. This curve is seen to be fairly close to the solid curve derived from the original Paris interaction. This provides an estimate of the faithfulness of the separable interaction (see also Ref. 4). The parametrization (A1) for the contribution of the HPW is the one that is used in the lower part of Fig. 12.

[1]C. Mahaux and R. Sartor, in *Nuclear Matter and Heavy-Ion Collisions,* edited by H. Flocard and M. Soyeur (Plenum, New York, in press).
[2]B. D. Day, Rev. Mod. Phys. **39**, 719 (1967).
[3]R. Sartor, Nucl. Phys. **A267**, 29 (1976).
[4]H. Lampl and M. K. Weigel, Phys. Rev. C **33**, 1834 (1986).
[5]J. Haidenbauer and W. Plessas, Phys. Rev. C **30**, 1822 (1984).
[6]M. Lacombe, B. Loiseau, J. M. Richard, R. Vinh Mau, J. Côté,

P. Pirès, and R. de Tourrreil, Phys. Rev. C **21**, 861 (1980).
[7]C. Mahaux, Nucl. Phys. **A328**, 24 (1979).
[8]T. T. S. Kuo and Z. Y. Ma, in *Nucleon-Nucleon Interaction and Nuclear Many Body Problems,* edited by S. S. Wu and T. T. S. Kuo (World Scientific, Singapore, 1984), p. 178.
[9]J. Hüfner and C. Mahaux, Ann. Phys. (N.Y.) **73**, 525 (1972).
[10]R. Sartor, Phys. Rev. C **30**, 2036 (1984).
[11]C. Mahaux and R. Sartor, Phys. Rev. C **19**, 229 (1978).
[12]N. M. Hugenholtz and L. Van Hove, Physica **24**, 363 (1958).
[13]J.-P. Jeukenne, A. Lejeune, and C. Mahaux, Phys. Rep. **25C**, 83 (1976).
[14]M. Baldo, I. Bombaci, L. Ferreira, G. Giansiracusa, and U. Lombardo, Phys. Lett. B **209**, 135 (1988).
[15]P. Grangé, J. Cugnon, and A. Lejeune, Nucl. Phys. **A473**, 365 (1987).
[16]K. A. Brueckner and D. T. Goldman, Phys. Rev. **117**, 207 (1960).
[17]H. S. Köhler, Phys. Rev. **137**, B1145 (1965).
[18]M. Baldo, I. Bombaci, G. Giansiracusa, and U. Lombardo, Phys. Rev. C **40**, R491 (1989).
[19]Xiangdong Ji and J. Engel, Phys. Rev. C **40**, R497 (1989).
[20]P. K. A. de Witt Huberts, in *Electron-Nucleus Scattering,* edited by A. Fabrocini, S. Fantoni, S. Rosati, and M. Viviani (World Scientific, Singapore, 1989), p. 349.
[21]B. D. Day, Phys. Rev. C **24**, 1203 (1981).
[22]S. Fantoni and V. R. Pandharipande, Nucl. Phys. **A427**, 473 (1984).
[23]B. D. Day and R. B. Wiringa, Phys. Rev. C **32**, 1057 (1985).
[24]R. Sartor and C. Mahaux, Phys. Rev. C **21**, 1546 (1980).
[25]J. G. Zabolitzky and W. Ey, Phys. Lett. **76B**, 527 (1978).
[26]J. W. Van Orden, W. Truex, and M. K. Banerjee, Phys. Rev. C **21**, 2628 (1980).
[27]M. Traini and G. Orlandini, Z. Phys. A **321**, 479 (1985).
[28]O. Benhar, C. Ciofi degli Atti, S. Liuti, and G. Salmè, Phys. Lett. B **177**, 135 (1986).
[29]C. Marchand, M. Bernhein, P. C. Dunn, A. Gérard, J. M. Laget, A. Magnon, J. Morgenstern, J. Mougey, J. Picard, U. Reffay-Pekeroen, S. Turck-Chieze, P. Vernin, M. K. Brussel, G. P. Capitani, E. De Sanctis, S. Frullani, and F. Garibaldi, in *Perspectives in Nuclear Physics at Intermediate Energies,* edited by S. Boffi, C. Ciofi degli Atti, and M. M. Giannini, (World Scientific, Singapore, 1988), p. 413.
[30]M. Jaminon, C. Mahaux, and H. Ngô, Nucl. Phys. **A452**, 445 (1986).
[31]R. D. Amado and R. M. Woloshyn, Phys. Rev. C **15**, 2200 (1977) and references contained therein.
[32]T. Cheon and E. F. Redish, Phys. Rev. C **39**, 331 (1989), and references contained therein.
[33]A. B. Migdal Zh. Eksp. Teor. Fiz. **32**, 399 (1957) [Sov. Phys.—JETP **5**, 333 (1957)].
[34]O. Bohigas and S. Stringari, Phys. Lett. **95B**, 9 (1980).
[35]M. Jaminon, C. Mahaux, and H. Ngô, Nucl. Phys. **A473**, 509 (1987).
[36]J.-P. Jeukenne, A. Lejeune, and C. Mahaux, Nucl. Phys. **A245**, 411 (1975).
[37]C. Mahaux, in *Jastrow versus Brueckner Theory,* Vol. 138 of *Lecture Notes in Physics,* edited by R. Guardiola and J. Ros (Springer Verlag, Berlin, 1981), p. 50.
[38]R. Sartor, Nucl. Phys. **A289**, 329 (1977).
[39]R. Sartor, Phys. Rev. C **27**, 899 (1983).
[40]C. Mahaux, Nucl. Phys. **A163**, 299 (1971).
[41]B. H. Brandow, Phys. Rev. **152**, 863 (1966).
[42]G. A. Baker, Jr. and J. L. Gammel, Phys. Rev. C **6**, 403 (1972).
[43]T. T. S. Kuo, Z. Y. Ma, and R. Vinh Mau, Phys. Rev. C **33**, 717 (1986); M. F. Jiang, T. T. S. Kuo, and H. Müther, *ibid.* **38**, 2408 (1988).
[44]C. Mahaux and R. Sartor, Phys. Rev. C **40**, 1833 (1989); M. F. Jiang, T. T. S. Kuo, and H. Müther, Phys. Rev. C **40**, 1836 (1989).
[45]B. D. Day, Rev. Mod. Phys. **50**, 495 (1978).
[46]E. N. M. Quint, B. M. Barnett, A. M. van den Berg, J. F. J. van den Brand, H. Clement, R. Ent, B. Frois, D. Goutte, P. Grabmayr, J. W. A. den Herder, E. Jans, G. J. Kramer, J. B. J. M. Lanen, L. Lapikàs, H. Nann, G. van der Steenhoven, G. J. Wagner, and P. K. A. de Witt Huberts, Phys. Rev. Lett. **58**, 1088 (1987).
[47]P. K. A. de Witt Huberts, Nucl. Phys. **A507**, 189c (1990).
[48]I. Sick, in *Electron-Nucleus Scattering,* edited by A. Fabrocini, S. Fantoni, S. Rosati, and M. Viviani (World Scientific, Singapore, 1989), p. 552.
[49]J. M. Cavedon, B. Frois, D. Goutte, M. Huet, Ph. Leconte, C. N. Papanicolas, H. H. Phan, S. K. Platchkov, S. Williamson, W. Boeglin, and I. Sick, Phys. Rev. Lett. **49**, 978 (1982).
[50]V. R. Pandharipande, C. N. Papanicolas, and J. Wambach, Phys. Rev. Lett. **53**, 1133 (1984).
[51]C. Mahaux and R. Sartor (unpublished).
[52]M. Razavy, Phys. Rev. **130**, 1091 (1963).